10

Effect of Fe_3O_4 nanoparticle concentration on the luminescence of $AgInS_2/ZnS$ in hybrid complex $CaCO_3$-Fe_3O_4@$AgInS_2/ZnS$

© D.A. Kurshanov, I.A. Arefina, M.S. Stepanova, A. Dubavik, A.V. Baranov

Center of Information Optical Technology, ITMO University, 197101 St. Petersburg, Russia

e-mail: kurshanov.danil@gmail.com

Received September 17, 2020
Revised July 14, 2021
Accepted July 21, 2021

In this paper, we studied the properties of a multifunctional system, in which the luminescent and magnetic properties are combined. The calcium carbonate microspheres are used as porous matrices for complexes combining luminescence properties of $AgInS_2/ZnS$ quantum dots and magnetic properties of Fe_3O_4 nanoparticles. The study investigates the effect of magnetic nanoparticles concentration on optical properties of quantum dots in $CaCO_3$-Fe_3O_4@$AgInS_2/ZnS$ complexes. It is shown that applying calcium carbonate microspheres as a matrix permits to reduce quenching of the quantum dots luminescence.

Keywords: hybrid system; ternary quantum dots, magnetic nanoparticles, iron oxide; calcium carbonate microspheres.

DOI: 10.21883/EOS.2022.14.53999.1418-21

Introduction

Recently, multifunctional or hybrid systems, which combine properties of different nanomaterials, have become prospective. Physical and chemical properties of nanoparticles allow for the creation of heterostructured materials with unique features. Such hybrid systems could be applied to a wide range of implementations for biomedicine, diagnostics, biological imaging, and a variety of sensor applications [1–4].

Among various possible combinations, optical and magnetic properties of materials can be distinguished. The multifunctional materials that combine luminescent and magnetic properties of nanomaterials within the same system offer promising prospects [5–7]. Similar multifunctional devices have advantages in biological fields as fluorescent imaging *in vitro* and *in vivo* and targeted drug delivery [7–9]. The synthesis of magneto-fluorescent materials requires obtaining particles with uniform and tunable size with high magnetic and luminescent properties as well as versatile surface functionalization with different radicals.

There are many different classes of magnetic materials, with the essential for the field of nanomedicine being superparamagnetic iron oxide nanoparticles formed by iron oxide nanocrystals with magnetite (Fe_3O_4) or maghemite (γ-Fe_2O_3) core. Magnetic iron oxide nanoparticles are widely used in cellular and molecular research and in magnetic resonance imaging [10–12].

The other class of inorganic nanoscale particles with luminescence properties are semiconductor quantum dots (QDs). Due to their diverse composition and unique photoluminescence characteristics as well as tunability of their optical properties as a result of quantum confinement, the QDs are one of the most interesting nanomaterials promising for using in hybrid systems [13]. The high photoluminescence (PL) quantum yield, high extinction coefficients in a wide spectral range, and photo- and chemical stability of QDs allow various applications, such as solar cells, LEDs, lasers, cell biology research, microscopy, and medical imaging applications [14–19].

Ternary I–III–VI QDs such as $CuInS_2$ and $AgInS_2$ are of special interest due to the absence of heavy metals such as Cd and Pb, and therefore being an alternative to the binary II–VI or IV–VI QDs. Ternary QDs have a large Stokes' shift and wide full-width at half-maximum (FWHM) [20], color-tunable emission in the region from 500 nm to near-infrared region [21–23], high quantum yield [24,25] and lifetime of the PL more than 100 ns [26,27].

In the present work, we use porous matrices of calcium carbonate microspheres to combine the luminescence properties of $AgInS_2/ZnS$ QDs and magnetic particles of Fe_3O_4. We also investigate the influence of Fe_3O_4 magnetic particles concentration on the optical properties of $AgInS_2/ZnS$ QDs in a solution and in a hybrid system.

Experimental

Materials

Ammonia hydrate (NH_4OH), indium(III) chloride ($InCl_3$), silver nitrate ($AgNO_3$), sodium sulfide ($Na_2S{\cdot}9H_2O$), thioglycolic acid (TGA), zinc(II) acetate dihydrate ($Zn(Ac)_2$), and isopropyl alcohol were used to synthesize $AgInS_2/ZnS$ QDs. Tris(acetylacetonato)iron(III), triethylene glycol (TEG), and tetrahydrofuran (THF) were used to synthesize Fe_3O_4 magnetic nanoparticles. Sodium carbonate (Na_2CO_3), calcium chloride ($CaCl_2$), poly(sodium 4-styrenesulfonate) sodium salt (PSS, Mw = 70 kDa) and poly(allylamine hydrochloride)

(PAH, Mw = 70 kDa) were used to synthesize $CaCO_3$ microspheres. All reagents purchased from Sigma-Aldrich, Steinheim, Germany, were used without further purification. In all procedures, deionized Hydrolab water was used.

Synthesis of $AgInS_2/ZnS$ QDs

$AgInS_2/ZnS$ QDs were synthesized by the hydrothermal method based on the reported procedure as follows [13]: 1 mL of $AgNO_3$ water solution (0.1 M), 2 mL of TGA water solution (1.0 M), and 0.2 mL of NH_4OH (5.0 M) were mixed in a three-necked round-bottom flask containing deionized water (92 mL) under room temperature and magnetic stirring. Then, 0.45 mL of NH_4OH solution (5.0 M) and 0.9 mL of 0.2 M HNO_3 solution with $InCl_3$ (1.0 M) were added. Next adding 1 mL of 1.0 M Na_2S water solution (1.0 M), the final solution was heated at 95°C for 30 min by a water bath. For ZnS shell growth on the surface of $AgInS_2$ cores, 1 mL of TGA solution (1.0 M) and 1 mL of 0.2 M HNO_3 solution with $Zn(Ac)_2$ (1.0 M) was added.

After the ZnS shell growth, the result $AgInS_2/ZnS$ QDs solution was cooled and concentrated using rotary evaporation. The size-selection procedure of nanoparticles was performed using a low relative amount of isopropyl alcohol and subsequent centrifugation at 10,000 rpm for 5 min. The precipitate was separated from the supernatant and dispersed in water. This procedure was repeated until the solution was fully discolored. In work, we used quantum dots with a luminescence peak at 620 nm.

Synthesis of Fe_3O_4 magnetic nanoparticles

Fe_3O_4 magnetic nanoparticles were synthesized by the thermal decomposition method: iron (III) triacetyl acetonate (1 mmol) was added in a three-necked round-bottom flask containing triethylene glycol (24 mL). The mixture was degassed under vacuum at 90°C for 60 min. After degassing, the system was filled with argon. Then the temperature was raised to 275°C and kept for 2 h under a constant argon flow. Afterwards, the mixture was cooled to room temperature by a water bath. The Fe_3O_4 magnetic nanoparticles were collected by centrifugation with THF and the precipitate was dissolved in water.

Synthesis of $CaCO_3$-Fe_3O_4@$AgInS_2/ZnS$ hybrid system

$CaCO_3$ microspheres were synthesized by mixing aqueous solutions Na_2CO_3 (0.33 M; 700 μL) and $CaCl_2 \cdot 2H_2O$ (0.33 M; 700 μL). Insertion of Fe_3O_4 nanoparticles into porous $CaCO_3$ microspheres was achieved by adding Fe_3O_4 aqueous solution during Na_2CO_3 and $CaCl_2 \cdot 2H_2O$ mixing. The amount of Fe_3O_4 magnetic nanoparticles varied from 10 to 160 μL (concentration of 1 mM). The mixture was stirred for 30 s, then the resulting spheres were centrifuged for 40 s at 3000 rpm. The precipitated $CaCO_3$-Fe_3O_4 microspheres were washed twice with H_2O.

The next step was the formation of the shell by the Layer-by-Layer (LbL) method. First, 1 mL of PAH solution (5 mg/mL, 0.5 M NaCl, pH 6.5) was added to the precipitated $CaCO_3$-Fe_3O_4 spheres, and dispersion was shaken for 10 min. The excess of PAH polyelectrolyte was removed by washing with water and centrifuging (30 s at 4000 rpm). Then, the next layer was covered by PSS solution (5 mg/mL, 0.5 M NaCl, pH 6.5). After triple coating with polymer layers (PAH/PSS/PAH), 50 μL of a QDs stock solution was added to the spheres. The dispersion was shaken for 10 min. The excess of QDs was removed by washing with water and centrifuging. The resulting $CaCO_3$-Fe_3O_4@$AgInS_2/ZnS$ hybrid system was dispersed in water.

Characterization of Materials

A spectrophotometer UV-3600 (Shimadzu, Kyoto, Japan) and spectrofluorometer FP-8200 (Jasco, Tokyo, Japan) were used for recording the absorption and PL spectra of the samples, respectively. Fluorescence images and local fluorescence spectra were carried out by LSM 710 (Zeiss, Oberkochen, Germany) confocal laser scanning fluorescence microscope based on an Axio Imager Z1 upright stand (Carl Zeiss Micro-Imaging) and a 20x/0.75 objective. A diode laser with a wavelength of 405 nm was used as an excitation source. Spectrally resolved samples images were recorded using a 32-channel photodetector, the spectral detection of which covers the entire visible wavelength range and provides a spectral step of 10 nm.

PL decay measurements were performed by laser scanning microscope MicroTime 100 (PicoQuant, Berlin, Germany), which allows recording the PL lifetimes in the range of 0.1−1000 ns with a time resolution up to 100 ps. Luminescence was excited by a semiconductor pulsed laser with a wavelength of 405 nm, pulse duration < 100 ps, and a pulse repetition rate up to 40 MHz. The average PL decay times of the samples were calculated using the formula $\langle \tau \rangle = \Sigma_i A_i \tau_i^2 / \Sigma_i A_i \tau_i$, where A_i and τ_i are the amplitude and decay time of the i-th component.

Results

Water-soluble $AgInS_2/ZnS$ QDs, which we used to obtain hybrid systems, were prepared in three steps: aqueous synthesis of $AgInS_2$ cores, shell growth ZnS and selective size separation. Size separation enables to get QDs with a luminescence peak at a wavelength from 550 to 650 nm due to the quantum confinement effect inherent in semiconductor nanostructures. We used QDs with luminescence maximum at 620 nm in this work. In Figure 1, *a, b*, the optical properties of the $AgInS_2/ZnS$ QDs are presented. In line with the previous reports [28], ternary QDs exhibit a broad emission band with a maximum at 620 nm and FWHM of 120 nm (405 nm excitation). The PL QY of the three QDs was estimated to be 32%. PL decay can be approximated by multi-exponential function with

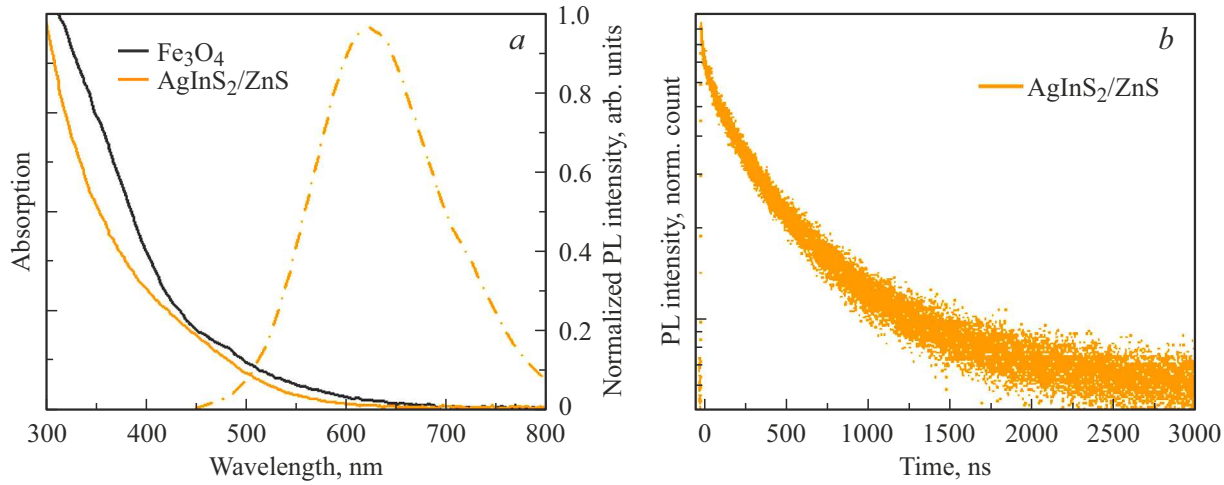

Figure 1. (*a*) Absorption (solid line) and PL spectra (dash-dotted line) of $AgInS_2/ZnS$ QDs (orange) and Fe_3O_4 magnetic nanoparticles (black); (b) PL decay curve of $AgInS_2/ZnS$ QDs. The measurements were performed at 405 nm excitation.

an average lifetime of 354 ± 8 ns. Such a long lifetime is a representative feature of ternary composition QDs and attributed to the domination of donor-acceptor pair recombination and the presence of intrinsic defect states in $AgInS_2$ nanoparticles [26,29].

For the magnetic nanoparticles, we used the decomposition process of an iron-containing precursor iron(III) acetylacetonate in an organic medium. For further experiments, Fe_3O_4 particles were precipitated with tetrahydrofuran and then dispersed in water. The absorption spectrum of the obtained samples is shown in Figure 1, *a*. The average size of Fe_3O_4 nanoparticles is approximately ~ 15 nm.

The next step was the investigation of the interaction between $AgInS_2/ZnS$ QDs and Fe_3O_4 magnetic nanoparticles in an aqueous solution. For this purpose, we added various volumes of magnetic nanoparticles with the concentration of 1mM (10, 20, 40, 80 and 160 μl) to the QDs solution. The optical properties of mixtures are shown in Figure 2. The increase of the magnetic Fe_3O_4 nanoparticles concentration leads to gradual decrease in the fluorescence intensity of $AgInS_2/ZnS$ QDs at 620 nm. The inset in Figure 2 shows the dependence of I/I_0 (where I and I_0 are PL intensity of $AgInS_2/ZnS$ QDS with the presence and absence of Fe_3O_4 nanoparticles, respectively) from the concentration of Fe_3O_4 nanoparticles. QDs PL quenching could be explained by several factors. The first one is the interaction between QDs and Fe_3O_4, which sharply decreases fluorescence at small distances between nanoparticles. Contact with the surface of a metal oxide particle results in electronic interaction and energy transfer [29,30]. The second is the broad absorption in the visible region of the spectrum by Fe_3O_4 nanoparticles that causes attenuation of the excitation light and the emitted QDs fluorescence [31,32].

In order to preserve the optical properties of $AgInS_2/ZnS$ QDs in a system with magnetic nanoparticles we used the following strategy to form $CaCO_3$-Fe_3O_4 complexes: (i) preparation of supersaturated Ca^{2+} and carbonate

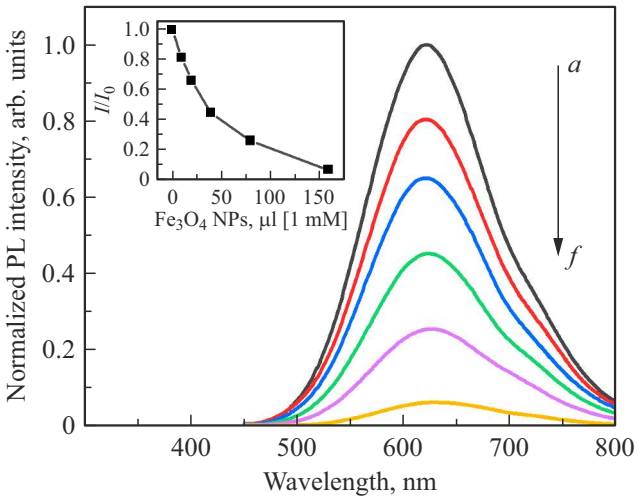

Figure 2. Normalized PL spectra of $AgInS_2/ZnS$ QDS in the presence of different concentrations of Fe_3O_4 in the range of 0–160 μl [1 mM]: *a*–*f* 0, 10, 20, 40, 80, 160 μl, respectively. The inset shows the dependence of I/I_0 from Fe_3O_4 additives, where I and I_0 are PL intensity of $AgInS_2/ZnS$ QDS with the presence of Fe_3O_4 nanoparticles and QDs PL intensity, respectively. The measurements were performed at 405 nm excitation.

solutions; (ii) fabrication of $CaCO_3$-Fe_3O_4 microspheres; (iii) coating the surface of microspheres with a triple layer of PAH/PSS/PAH polyelectrolytes, as shown in Figure 3, *a*. Totally five samples were obtained in which the concentration of magnetic Fe_3O_4 nanoparticles changes with a concentration of 1 mM in the range from 10 to 160 μl (10/20/40/80/160 μl).

The morphology and average size of $CaCO_3$-Fe_3O_4 microspheres were investigated by the confocal laser scanning fluorescence microscope (Figure 3, *b*). $CaCO_3$ exists as one of some anhydrous crystalline polymorphs: rhomboidal calcite, needle-like aragonite, and spherical vaterite. The

Lifetimes and normalized amplitudes of $AgInS_2/ZnS$ QDs and fluorescent $CaCO_3$-Fe_3O_4@$AgInS_2/ZnS$ complexes with different concentrations of Fe_3O_4 in the range of 0–160 μl [1 mM]: 0-5 0, 10, 20, 40, 80, 160 μl, respectively

Samples	a_1	τ_1	a_2	τ_2	a_3	τ_3	$\langle\tau\rangle$
$AgInS_2/ZnS$	0.31 ± 0.02	451 ± 9	0.43 ± 0.02	245 ± 14	0.21 ± 0.01	29 ± 5	554 ± 8
0	0.110 ± 0.004	416 ± 8	0.26 ± 0.01	83 ± 4	0.53 ± 0.02	8.1 ± 0.7	293 ± 3
1	0.59 ± 0.01	428 ± 6	1.73 ± 0.03	89 ± 2	4.2 ± 0.2	8.8 ± 0.6	274 ± 2
2	0.060 ± 0.004	443 ± 15	0.23 ± 0.01	101 ± 4	0.38 ± 0.01	14 ± 1	255 ± 2
3	0.24 ± 0.01	438 ± 6.1	0.96 ± 0.02	88 ± 3	3.2 ± 0.1	8.2 ± 0.4	250 ± 2
4	0.48 ± 0.01	433 ± 4	2.09 ± 0.05	89 ± 2	6.1 ± 0.2	9.8 ± 0.5	237 ± 1
5	0.15	413 ± 8	0.81 ± 0.01	92 ± 2	1.81 ± 0.05	13 ± 1	203 ± 1

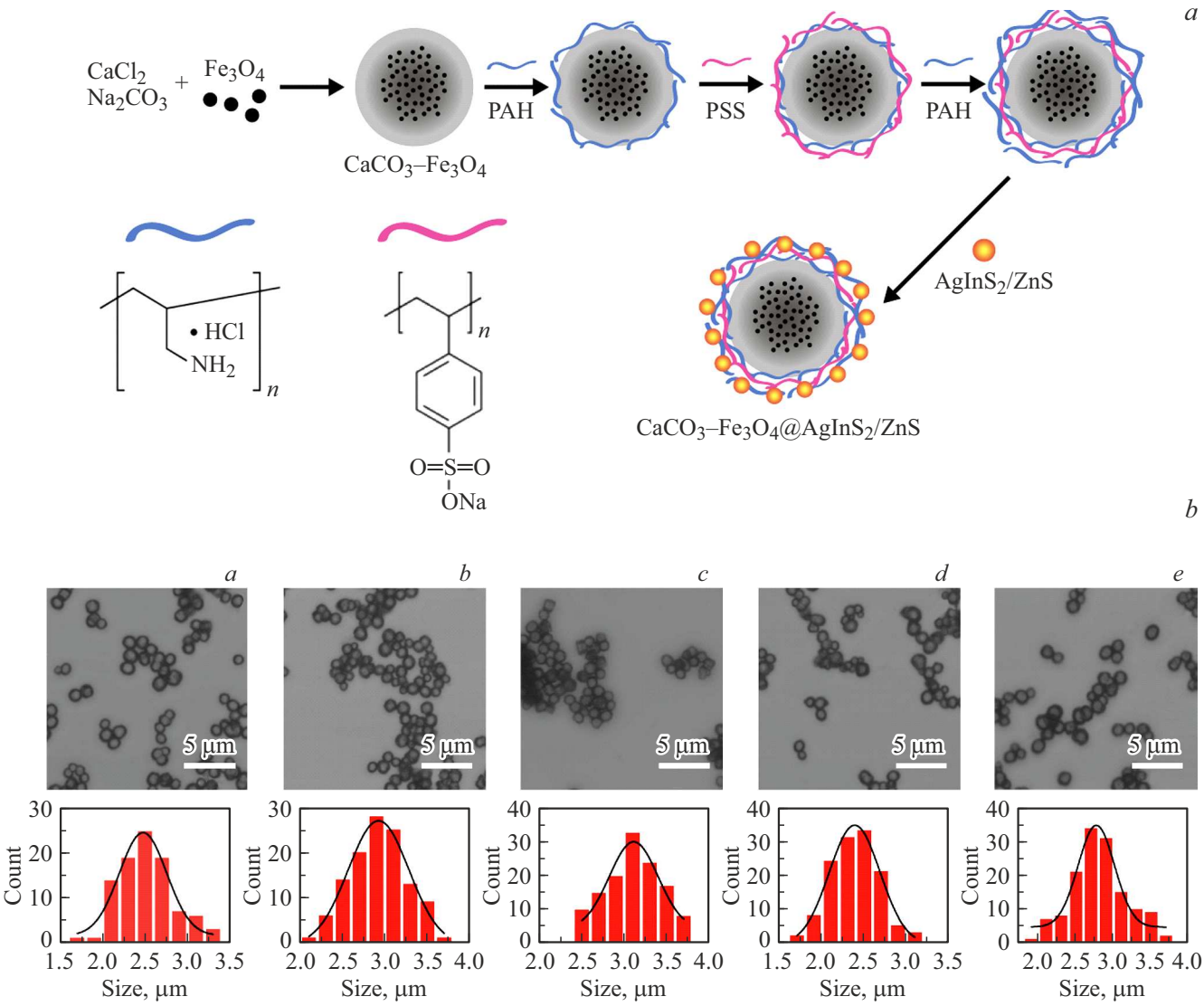

Figure 3. (*a*) Scheme of synthesis and LbL process of forming the $CaCO_3$-Fe_3O_4@$AgInS_2/ZnS$ complexes. (*b*) An overlay of the transmitted light imaged by confocal fluorescence microscopy of the $CaCO_3$-Fe_3O_4@$AgInS_2/ZnS$ complexes with different concentrations of Fe_3O_4 in the range of 0–160 μl [1 mM]: *a*–*e* 0, 10, 20, 40, 80, 160 μl, respectively. The histograms of the size distribution of microspheres were elaborated by measuring the particle sizes from the confocal images. Scale bars are 5 μm for images.

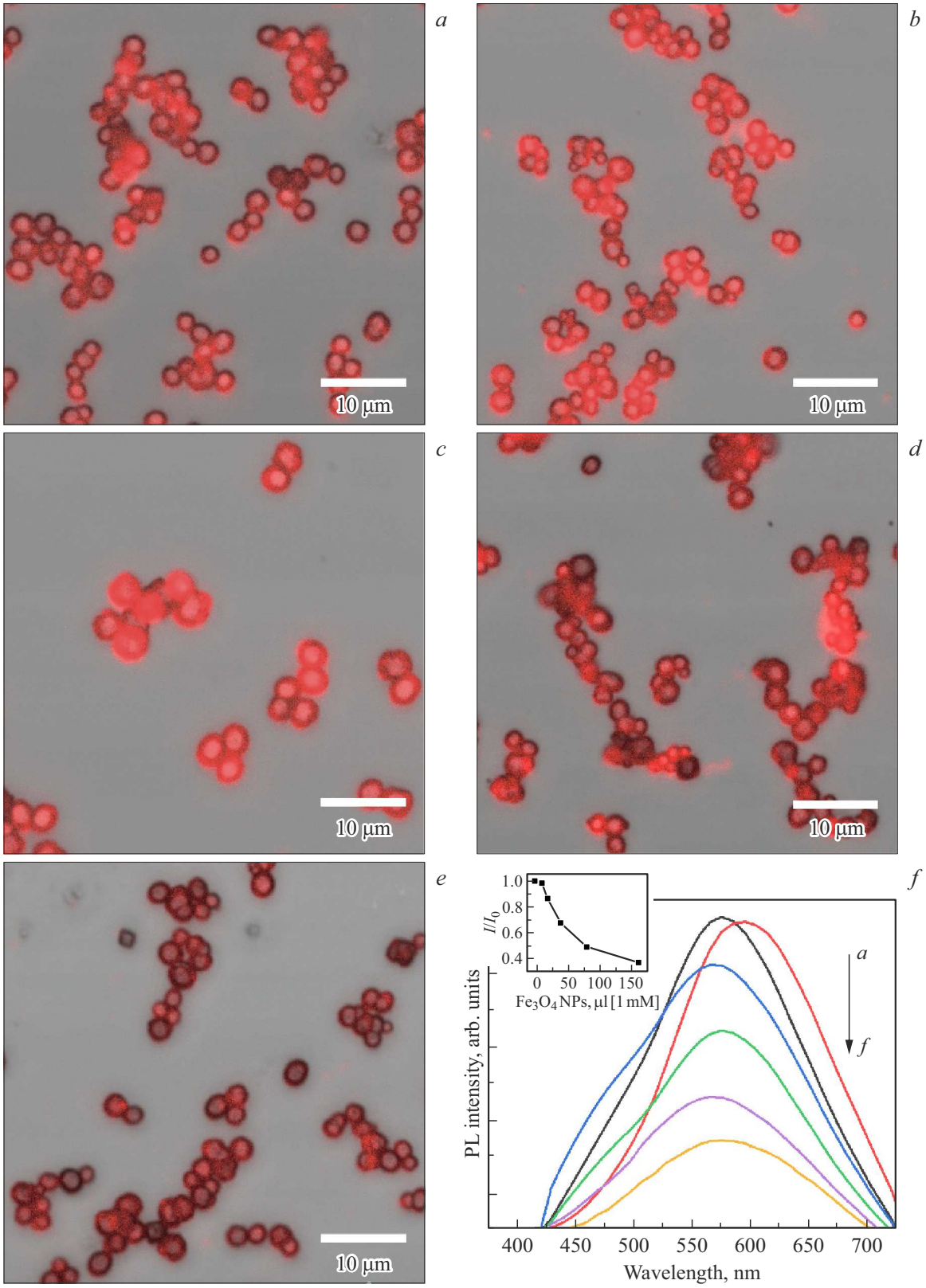

Figure 4. (*a*–*e*) Overlay of the microscopic images of complexes with different concentrations of Fe_3O_4 in the range of 10–160 μl [1 mM]: *a*–*e* 10, 20, 40, 80, 160 μl, respectively, in transmission and luminescent channels artificially colored in red. Scale bars are 10 μm. (*f*) PL spectra of samples with different concentrations of Fe_3O_4 in the range of 0–160 μl [1 mM]: *a*–*f* 0, 10, 20, 40, 80, 160 μl, respectively. The inset shows the dependence of I/I_0 from Fe_3O_4 additives, where I and I_0 are PL intensity of $AgInS_2$/ZnS QDs with the presence of Fe_3O_4 nanoparticles and PL intensity of pristine QDs, respectively.

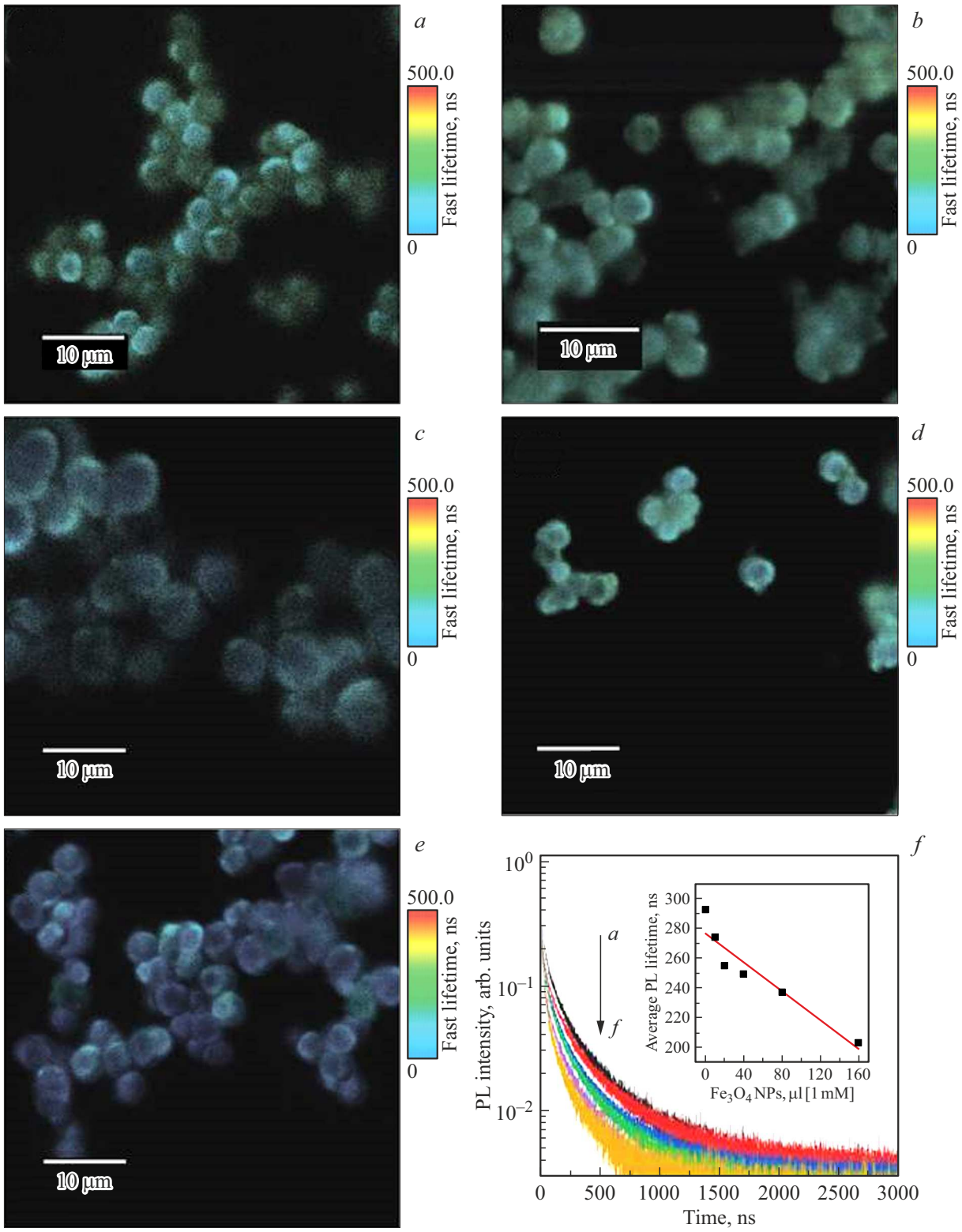

Figure 5. (*a*–*e*) FLIM images by time-resolved confocal fluorescence microscope of the $CaCO_3$-Fe_3O_4@$AgInS_2$/ZnS complexes (Fe_3O_4 in the range of 0–160 μl [1 mM]: *a*–*e* 0, 10, 20, 40, 80, 160 μl, respectively). Scale bars are 10 μm for images. (*f*) PL decay curves of samples with different concentrations of Fe_3O_4 in the range of 0–160 μl [1 mM]: *a*–*f* 0, 10, 20, 40, 80, 160 μl, respectively. The inset shows the dependence of average PL lifetimes of complexes from Fe_3O_4 magnetic nanoparticles concentration.

investigations demonstrated the formation of micro-sized spheres $CaCO_3$ with an average size of $2.4-3.1\,\mu$m. The morphology of this type is a characteristic of polymorphic modification of $CaCO_3$ vaterite. The spherical shape of vaterite has a porous internal structure that allows the use in various biomedical applications as a system for encapsulation, transportation, and controlled release of molecules of therapeutic interest (drug delivery) [33–35].

$AgInS_2$/ZnS QDs stabilized with TGA were deposed on the microspheres surface by electrostatic interaction between the outer positive PAH polyelectrolyte layer on the surface of microspheres and negative thiol groups on the surface of $AgInS_2$/ZnS QDs [36]. $AgInS_2$/ZnS QDs were added in excess to $CaCO_3$-Fe_3O_4 complexes, non-joined dots were removed, and the obtained complexes were washed with distilled water.

The optical properties of the obtained $CaCO_3$-Fe_3O_4@$AgInS_2$/ZnS complexes were studied by the confocal microscope at a wavelength of 405 nm and laser scanning confocal microscope (PicoQuant). An overlay of the transmitted light and fluorescent channel in artificial (red) color are presented in Figure 4, *a–e*. The images confirm that the QDs are distributed evenly on the surface of the $CaCO_3$-Fe_3O_4 microspheres. The PL spectra of microspheres on a glass substrate and pure $AgInS_2$/ZnS QDs in an aqueous solution are shown in Figure 4, *f*. Their spectra demonstrate a broad luminescence band similar to that of pure $AgInS_2$/ZnS QDs. We observe a small PL blue shift of ternary QDs in polymer layers on the surface of $CaCO_3$-Fe_3O_4 microspheres. As with solutions of QDs and magnetic nanoparticles the fluorescence intensity decrease of $AgInS_2$/ZnS QDs in complexes $CaCO_3$-Fe_3O_4@$AgInS_2$/ZnS. However, large concentrations of Fe_3O_4 do not lead to complete $AgInS_2$/ZnS PL quenching.

The PL decay lifetimes of $CaCO_3$-Fe_3O_4@$AgInS_2$/ZnS complexes with different concentrations of magnetic nanoparticles were measured by time-resolved confocal fluorescence microscope MicroTime200. To complement the above measurements by the confocal microscope, fluorescence lifetime imaging microscopy (FLIM) mapping was completed of the $CaCO_3$-Fe_3O_4@$AgInS_2$/ZnS complexes. Figure 5, *a* presents the FLIM images of the samples received. The images show the spherical shape of complexes and confirm that all samples exhibit a spatial homogeneity in PL lifetimes.

The change of PL decay lifetimes is demonstrated in Table. The PL decay of the $CaCO_3$-Fe_3O_4@$AgInS_2$/ZnS complexes was approximated by a multi-exponential function, as well as in the case of $AgInS_2$/ZnS QDs aqueous solution. The average PL lifetimes of $AgInS_2$/ZnS QDs on surface microspheres reduced by almost a factor of 10% in comparison to pure $AgInS_2$/ZnS QDs. Additionally, the PL lifetimes decrease with increasing concentration of Fe_3O_4 magnetic nanoparticles in complexes, with values changing between 300 and 225 ns from 10 to 160 μl (1 mM), respectively. Such changes in average PL lifetimes indicate an increase in the number of nonradiative relaxation transitions due to the interaction of $AgInS_2$/ZnS QDs with the matrix of complexes and energy transfer between Fe_3O_4 and $AgInS_2$/ZnS.

Conclusion

In this work, we have obtained the complexes based on microspheres of calcium carbonate with the luminescence and magnetic properties. The loading of Fe_3O_4 magnetic nanoparticles in a porous microsphere of $CaCO_3$ and coating surface polyelectrolytes and $AgInS_2$/ZnS QDs allows retaining the physicochemical properties of system components. By changing Fe_3O_4 nanoparticles concentration, PL intensity changes of $AgInS_2$/ZnS QDs were observed in solution and in hybrid complexes. However, loading magnetic particles into the porous structure of calcium carbonate permits to reduce quenching of the quantum dots luminescence. This leads to increasing the loading limit of magnetic particles and increasing the system's magnetic properties while forming complexes that possess luminescence and magnetism. Our research on the optical properties of the $CaCO_3$-Fe_3O_4@$AgInS_2$/ZnS complexes contributes to the further developing hybrid systems for nano- and biotechnology implications.

Funding

This research was funded by the RFBR, project number 19-33-90250.

Conflicts of Interest

The authors declare no conflict of interest.

References

[1] C. Wang, P. Makvandi, E.N. Zare, F.R. Tay, L. Niu. Advanced Therapeutics, **3**, 2000024 (2020).
[2] G. Yu, J. Yang, X. Fu, Z. Wang, L. Shao, Z. Mao, Y. Liu, Z. Yang, F. Zhang, W. Fan, J. Song, Z. Zhou, C. Gao, F. Huang, X. Chen. Mater. Horiz., **5**, 429 (2018).
[3] M. Venkateswarulu, D. Gambhir, H. Kaur, P.V. Daniel, P. Mondal, R.R. Koner. Dalton Trans., **46**, 13118 (2017).
[4] L. Jothi, N. Jayakumar, S.K. Jaganathan, G. Nageswaran. Materials Research Bulletin, **98**, 300 (2018).
[5] Y. Ma, Y. Zhong, J. Fan, W. Huang. Mater. Res. Express **5**, 035025 (2018).
[6] I.V. Zelepukin, V.O. Shipunova, A.B. Mirkasymov, P.I. Nikitin, M.P. Nikitin, S.M. Deyev. in 2018 International Conference Laser Optics (ICLO) (IEEE, St. Petersburg, 2018), pp. 576–576.
[7] Q. Wu, Y. Lin, F. Wo, Y. Yuan, Q. Ouyang, J. Song, J. Qu, and K.-T. Yong. Small, **13**, 1701129 (2017).
[8] L. Xia, X. Li, F. Zhu, S. Hu, and L. Huang. J. Phys. Chem. C, **121**, 20279 (2017).
[9] X. Liang, J. Fan, Y. Wang, Y. Zhao, R. Jin, T. Sun, M. Cheng, X. Wang. Journal of Rare Earths **35**, 419 (2017).

[10] Wahajuddin, S. Arora. IJN **7**, 3445 (2012).
[11] C. Justin, S.A. Philip, A.V. Samrot. Appl Nanosci, **7**, 463 (2017).
[12] Y. Huang, K. Mao, B. Zhang, Y. Zhao. Materials Science and Engineering, C, **70**, 763 (2017).
[13] A. Raevskaya, V. Lesnyak, D. Haubold, V. Dzhagan, O. Stroyuk, N. Gaponik, D.R.T. Zahn, A. Eychmüller. J. Phys. Chem. C, **121**, 9032 (2017).
[14] Q. Pei, Z. Chen, S. Wang, D. Zhang, P. Ma, S. Li, X. Zhou, Y. Lin. Solar Energy, **178**, 108 (2019).
[15] B. Samuel, S. Mathew, V.R. Anand, A.A. Correya, V.P.N. Nampoori, A. Mujeeb. Mater. Res. Express, **5**, 025009 (2018).
[16] N. Ming, S. Tao, W. Yang, Q. Chen, R. Sun, C. Wang, S. Wang, B. Man, H. Zhang, Opt. Express. OE, **26**, 9017 (2018).
[17] G. Gao, Y.-W. Jiang, W. Sun, F.-G. Wu. Chinese Chemical Letters, **29**, 1475 (2018).
[18] S. Sarkar, P. Le, J. Geng, Y. Liu, Z. Han, M.U. Zahid, D. Nall, Y. Youn, P.R. Selvin, and A.M. Smith. J. Am. Chem. Soc., **142**, 3449 (2020).
[19] D.V. Freitas, S.G.B. Passos, J.M.M. Dias, A. Mansur, S.M. Carvalho, H. Mansur, M. Navarro. Sensors and Actuators B: Chemical, **250**, 233 (2017).
[20] A.S. Baimuratov, I.V. Martynenko, A.V. Baranov, A.V. Fedorov, I.D. Rukhlenko, and S.Yu. Kruchinin. J. Phys. Chem. C, **123**, 16430 (2019).
[21] C. Cai, L. Zhai, Y. Ma, C. Zou, L. Zhang, Y. Yang, S. Huang, Journal of Power Sources, **341**, 11 (2017).
[22] L. Liu, R. Hu, W.-C. Law, I. Roy, J. Zhu, L. Ye, S. Hu, X. Zhang, K.-T. Yong, Analyst. **138**, 6144 (2013).
[23] B. Mao, C.-H. Chuang, C. McCleese, J. Zhu, C. Burda. J. Phys. Chem. C, **118**, 13883 (2014).
[24] D. Su, L. Wang, M. Li, S. Mei, X. Wei, H. Dai, Z. Hu, F. Xie, R. Guo. Journal of Alloys and Compounds, **824**, 153896 (2020).
[25] W. Xiang, C. Xie, J. Wang, J. Zhong, X. Liang, H. Yang, L. Luo, and Z. Chen. Journal of Alloys and Compounds, **588**, 114 (2014).
[26] B. Mao, C.-H. Chuang, J. Wang, C. Burda, J. Phys. Chem. C, **115**, 8945 (2011).
[27] Y.J. Park, J.H. Oh, N.S. Han, H.C. Yoon, S.M. Park, Y.R. Do, J.K. Song, J. Phys. Chem., C, **118**, 25677 (2014).
[28] Y. Gromova, A. Sokolova, D. Kurshanov, I. Korsakov, V. Osipova, S. Cherevkov, A. Dubavik, V. Maslov, T. Perova, Y. Gun'ko, A. Baranov, A. Fedorov, Materials **12**, 3616 (2019).
[29] M. Dai, S. Ogawa, T. Kameyama, K. Okazaki, A. Kudo, S. Kuwabata, Y. Tsuboi, T. Torimoto. J. Mater. Chem., **22**, 12851 (2012).
[30] X. Hong, J. Li, M. Wang, J. Xu, W. Guo, J. Li, Y. Bai, T. Li. Chem. Mater. **16**, 4022 (2004).
[31] T.R. Sathe, A. Agrawal, S. Nie. Anal. Chem. **78**, 5627 (2006).
[32] Z. Liu, G. Li, T. Xia, X. Su. Sensors and Actuators B: Chemical, **220**, 1205 (2015).
[33] L. Pérez-Villarejo, F. Takabait, L. Mahtout, B. Carrasco-Hurtado, D. Eliche-Quesada, P.J. Sánchez-Soto. Ceramics International **44**, 5291 (2018).
[34] D.B. Trushina, T.V. Bukreeva, M.V. Kovalchuk, M.N. Antipina. Materials Science and Engineering: C, **45**, 644 (2014).
[35] Y. Boyjoo, V.K. Pareek, J. Liu. J. Mater. Chem. A **2**, 14270 (2014).
[36] O.S. Oluwafemi, B.M.M. May, S. Parani, J.V. Rajendran, Journal of Materials Research, **34**, 4037 (2019).